applied optics

Two-dimensional refractive index modulation by phased array transducers in acousto-optic deflectors

Tiansi Wang,[1] Chong Zhang,[2] Aleksandar Aleksov,[3] Islam Salama,[2] and Aravinda Kar[4,*]

[1]CREOL, The College of Optics & Photonics, University of Central Florida, P.O. Box 162700, Orlando, Florida 32816-2700, USA
[2]Intel—Assembly & Test Technology Development, 5000 W Chandler Blvd., Chandler, Arizona 85226, USA
[3]Intel—Components Research, 5000 W Chandler Blvd., Chandler, Arizona 85226, USA
[4]CREOL, The College of Optics & Photonics, Mechanical and Aeronautical Engineering and Material Science Engineering Department, University of Central Florida, P.O. Box 162700, Orlando, Florida 32816-2700, USA
*Corresponding author: akar@creol.ucf.edu

Received 26 September 2016; revised 14 December 2016; accepted 22 December 2016; posted 22 December 2016 (Doc. ID 276539); published 19 January 2017

Acousto-optic deflectors are photonic devices that are used for scanning high-power laser beams in advanced microprocessing applications such as marking and direct writing. The operation of conventional deflectors mostly relies on one-dimensional sinusoidal variation of the refractive index in an acousto-optic medium. Sometimes static phased array transducers, such as step configuration or planar configuration transducer architecture, are used to tilt the index modulation planes for achieving higher performance and higher resolution than a single transducer AO device. However, the index can be modulated in two dimensions, and the modulation plane can be tilted arbitrarily by creating dynamic phase gratings in the medium using phased array transducers. This type of dynamic two-dimensional acousto-optic deflector can provide better performance using, for example, a large deflection angle and high diffraction efficiency. This paper utilizes an ultrasonic beam steering approach to study the two-dimensional strain-induced index modulation due to the photoelastic effect. The modulation is numerically simulated, and the effects of various parameters, such as the operating radiofrequency of the transducers, the ultrasonic beam steering angle, and different combinations of pressure on each element of the transducer array, are demonstrated.

OCIS codes: (230.1950) Diffraction gratings; (230.1040) Acousto-optical devices.

https://doi.org/10.1364/AO.56.000688

1. INTRODUCTION

The scanning or deflection of light with high performance and broad frequency bandwidth is applied in a number of applications, including light modulators, optical beam deflectors, optical signal processors, optical tunable filters [1,2], radiofrequency (RF) spectrum analyzers [3], wavelength division multiplexing optical communication [4–6], optical tweezers for molecule trapping [7–9], optical image scanners [10–12], optical fringe pattern projectors [13–15], and optical frequency shifters [16,17]. Acousto-optic deflectors (AODs) involve interactions between lasers and acoustic waves, and the deflectors generally operate in three different modes: random access, continuous mode, and multi-frequency modes [18]. The performance of the AODs is characterized by the angular resolution for deflecting the laser beam, the acoustic frequency bandwidth for modulating the phase grating in the AOD medium, the diffraction efficiency to maximize the laser power in the first order diffracted laser beam, and the access time to minimize the time for the deflector to steer the beam from one position to another one. The access time, which is the ratio of the laser beam diameter to the acoustic velocity, represents the necessary time for the acoustic wave to propagate through the laser beam.

Therefore, the operation of AODs using ultrasonic longitudinal or shear waves impacts the performance of the deflector. The longitudinal waves (L-waves) successively compress and stretch the distance between the atomic planes of the AOD material in the direction of the ultrasonic wave propagation, which is similar to the compression and rarefaction phenomena caused by sound waves in air. The shear waves (S-waves), on the other hand, vibrate the atoms at right angles to the direction of the ultrasonic wave propagation. Since the velocity of L-waves is generally much higher than that of the S-waves, the L-waves allow shorter access time and, consequently, make the deflectors faster than the S-wave mode of operation. The lower velocity of

S-waves, however, yields a larger deflection angle than in the case of L-waves.

The diffraction efficiency and the deflection scan angle are governed by the elasto-optic or photoelastic effect, which states that mechanical stresses modify the refractive index. This effect arises when acoustic waves propagate through a medium since an acoustic wave is a traveling strain or pressure disturbance in the material. Acoustic waves, therefore, can be considered as time-varying deformations of atomic planes in the acousto-optic medium with displaced particles from their equilibrium positions. This mechanical effect of acoustic waves modifies the refractive index of the medium in a periodic pattern and produces a dynamic volume phase grating for the laser light passing through the medium. The displacement of the particles can be determined by solving the Christoffel equation that involves the tensor constitutive relation of the material properties [18]. Nakahata and Kono [19] simplified this equation to express the diffraction of acoustic waves as a modified Rayleigh–Sommerfeld integral (mRSI) for the particle displacement vector field, and evaluated the integral numerically to analyze ultrasonic beam steering by phased array transducers. The applications of the phased array technology for beam steering include non-destructive testing of material defects, radar, underwater acoustics, medical diagnostics, and therapeutic treatment. Wang *et al.* [20] evaluated the mRSI analytically for transducers of small widths to obtain the displacement vector field that compares well with the numerical solution of the integral [19]. The analytic expression of the integral is used in this study to determine the strain induced in the acousto-optic medium by phased array piezoelectric transducers, and then the two-dimensional variation of the refractive index is calculated using the strain tensor.

2. ANALYTIC MODEL

A. Strain Tensor in the AOD Medium Due to a Row of Phased Array Transducers

In this study, a row of transducers is attached to the AOD medium at the surface $z = 0$ as shown in Fig. 1. The width and length of each transducer are $2a$ and infinite along the x and y axes, respectively. For each transducer, if P_0 is the pressure exerted on the AOD, c_l is the speed of L-waves in the AOD, and κ and α are the wave number and attenuation coefficients of the waves, respectively, the displacement vector of the atoms in the AOD medium can be written as follows for the unit length of the medium along the y axis [20]:

$$\text{for } x \neq x_{\text{cm}}$$

$$\vec{U}(x,z) = -\frac{P_0}{2\pi\rho c_l^2}\frac{1}{i(\kappa+i\alpha)} \times \sum_{m=1}^{M} A_m \frac{\exp[i(\kappa+i\alpha)b_u] - \exp[i(\kappa+i\alpha)b_l]}{x - x_{\text{cm}}} \quad (1)$$

and for $x = x_{\text{cm}}$

$$\vec{U}(x,z) = \frac{P_0 a}{\pi\rho c_l^2}\frac{1}{\sqrt{z^2+a^2}}\sum_{m=1}^{M} A_m \exp(i(\kappa+i\alpha)\sqrt{z^2+a^2}), \quad (2)$$

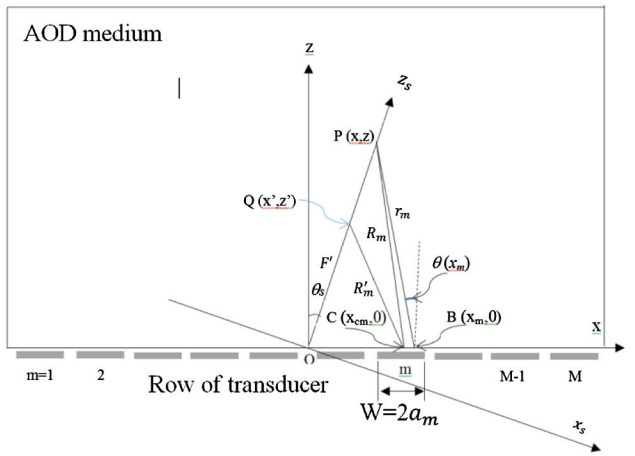

Fig. 1. Schematic of coordinate system for a modeling of a contact phased array transducer located on solid AO medium.

where the two integration limits are defined as $b_l = \sqrt{z^2 + [x - (x_{\text{cm}} - a)]^2}$, $b_u = \sqrt{z^2 + [x - (x_{\text{cm}} + a)]^2}$ and x_{cm} is the coordinate of the center of the mth transducer on the x axis; i.e., x_{cm} is negative when the transducer is on the $-x$ axis. The expression for A_m is given by $A_m = D(\theta(x_{\text{cm}}))\vec{d}_p(x_{\text{cm}})\exp(i\Delta\phi_m)$ with the following definitions of the variables.

Directivity function due to mth transducer:

$$D(\theta(x_m)) = \frac{c^2\left(\frac{1}{2}c^2 - \sin^2\theta(x_m)\right)\cos\theta(x_m)}{2(\sin^2\theta(x_m) - c^2/2)^2 + \frac{1}{2}\sin^2(2\theta(x_m))\sqrt{c^2 - \sin^2\theta(x_m)}} \quad (3)$$

Polarization vector due to mth transducer:

$$\vec{d}_p(x_m) = \frac{x - x_m}{\sqrt{(x-x_m)^2 + z^2}}\hat{x} + \frac{z}{\sqrt{(x-x_m)^2 + z^2}}\hat{z}. \quad (4)$$

The phase shift due to the time delay, $\Delta\tau_m$, for ultrasonic waves arriving at point $Q(x', z')$ from points $C(x_{\text{cm}}, 0)$ and $O(0, 0)$, i.e., $\Delta\tau_m = (F' - R'_m)/c_l$, where Q is the point of focus at a distance F' from the point O, and R'_m is the distance CQ [19,21] is given by the following expression:

$$\Delta\phi_m = 2\pi F\Delta\tau_m = \frac{2\pi}{\Lambda}F'[1 - \{F'^2 + x_{\text{cm}}^2 - 2F'x_{\text{cm}}\sin\theta_s\}^{1/2}]. \quad (5)$$

Here $\theta(x_m)$ is the angular position of the point of interest $P(x, z)$ in the AOD medium relative to the normal to the surface of the mth transducer at an arbitrary point B $(x_m, 0)$; i.e., $\theta(x_m)$ is the angle between this normal and the line BP, and c is the ratio of the speeds of ultrasonic L-waves to the S-waves. $\hat{x}$ and $\hat{z}$ are the unit vectors along the x and z axes, respectively. F and Λ are the frequency and wavelength in the AOD medium for the ultrasonic waves generated by each transducer, and θ_s is the steering angle, which is taken to be positive when measured from the z axis in the clockwise direction.

Equations (1) and (2) yield the displacement vector $\vec{U}(x, z) = u_x(x, z)\hat{x} + u_z(x, z)\hat{y}$, where $u_x(x, z)$ and $u_z(x, z)$

are the displacement components in the x and z directions, respectively. Using these components, the deformation inside the AOD medium can be characterized by the displacement gradient $\frac{\partial u_i}{\partial x_j}$, where the indices $i, j = 1, 2, 3$ are the coordinates x, y, z, respectively. The mechanical strains due to this deformation are represented by a second-rank strain tensor, $\boldsymbol{S} = [S_{ij}]$, and each strain component is given by the following expression [18,22]:

$$S_{ij} = \frac{1}{2}\left(\frac{\partial u_i}{\partial x_j} + \frac{\partial u_j}{\partial x_i}\right). \tag{6}$$

This strain changes the atomic density within the volume of acoustic wave propagation inside the AOD and, consequently, modifies the refractive index.

B. Two-Dimensional Refractive Index Due to Photoelastic Effect

Equation (7) is used to determine the refractive index based on the photoelastic effect. The refractive index is inversely related to the relative impermeability tensor, and this tensor depends on the strain tensor by the following expression [23]:

$$\eta_{ij}(\boldsymbol{S}) = \eta_{iju} + \Delta\eta_{ij}(\boldsymbol{S}) = \eta_{iju} + \sum_{k,l} p_{ijkl} S_{kl}, \tag{7}$$

where η_{iju} is the relative impermeability tensor of the unstrained medium, $\Delta\eta_{ij}(\boldsymbol{S})$ is the change in the relative impermeability tensor due to strain, and p_{ijkl} represents the dimensionless photoelastic coefficient as a fourth-rank tensor. Since the photoelastic tensor is symmetric in i and j, and in k and l, the indices can be contracted to simplify the double indices ij and kl to single indices g and h, respectively, as follows:

$$p_{ijkl} = p_{jikl} = p_{ijlk} = p_{jilk} = p_{gh}, \tag{8}$$

where each of $i, j, k, l = 1, 2, 3$ and each of $g, h = 1, 2, 3, 4, 5, 6$. Therefore, Eq. (7) can be expressed as

$$\begin{bmatrix}\eta_1\\ \eta_2\\ \eta_3\\ \eta_4\\ \eta_5\\ \eta_6\end{bmatrix} = \begin{bmatrix}\eta_{1u}\\ \eta_{2u}\\ \eta_{3u}\\ \eta_{4u}\\ \eta_{5u}\\ \eta_{6u}\end{bmatrix} + \begin{bmatrix}p_{11} & p_{12} & p_{13} & p_{14} & p_{15} & p_{16}\\ p_{21} & p_{22} & p_{23} & p_{24} & p_{25} & p_{26}\\ p_{31} & p_{32} & p_{33} & p_{34} & p_{35} & p_{36}\\ p_{41} & p_{42} & p_{43} & p_{44} & p_{45} & p_{46}\\ p_{51} & p_{52} & p_{53} & p_{54} & p_{55} & p_{56}\\ p_{61} & p_{62} & p_{63} & p_{64} & p_{65} & p_{66}\end{bmatrix}\begin{bmatrix}s_1\\ s_2\\ s_3\\ s_4\\ s_5\\ s_6\end{bmatrix}, \tag{9}$$

where the strain elements S_h are defined by the following rule:

$$\begin{bmatrix}S_1\\ S_2\\ S_3\\ S_4\\ S_5\\ S_6\end{bmatrix} = \begin{bmatrix}S_{xx}\\ S_{yy}\\ S_{zz}\\ 2S_{yz}\\ 2S_{xz}\\ 2S_{xy}\end{bmatrix}. \tag{10}$$

The variation of refractive index at different points in the presence of a strain field is given by an index ellipsoid:

$$X^2\left(\frac{1}{n_u^2} + \Delta\eta_1\right) + Y^2\left(\frac{1}{n_u^2} + \Delta\eta_2\right) + Z^2\left(\frac{1}{n_u^2} + \Delta\eta_3\right) + 2YZ\Delta\eta_4 + 2XZ\Delta\eta_5 + 2XY\Delta\eta_6 = 1, \tag{11}$$

where X, Y, and Z are not the usual Cartesian coordinates but dimensionless electric displacement components in the x, y, and z directions, respectively. $X = \frac{D_x}{\sqrt{2\varepsilon_0\tilde{U}}}$, $Y = \frac{D_y}{\sqrt{2\varepsilon_0\tilde{U}}}$, and $Z = \frac{D_z}{\sqrt{2\varepsilon_0\tilde{U}}}$ with D_x, D_y, and D_z as the x, y, and z components, respectively, of the electric displacement field $\boldsymbol{D}$ corresponding to the electric field ($\boldsymbol{E}$) of the laser beam; ε_0 is the permittivity of vacuum; and the energy density $\tilde{U} = \frac{1}{2}\boldsymbol{E}\cdot\boldsymbol{D}$. Since the photoelastic constants p_{ij} are defined in the crystal coordinate system, the x, y, z coordinate system of this study is chosen to coincide with one of the commonly grown crystal growth axes for supporting the L-mode propagation; i.e., the x, y, and z axes are parallel to the [100], [010], and [001] directions, respectively. Kastelik *et al.* [24] introduced a spreading parameter for the propagation of acoustic S-modes in TeO_2 and showed that this parameter is not unity for anisotropic media. In the present study, this parameter is taken as unity, which holds good for isotropic media.

To determine the variation of the refractive index in the principal directions, Eq. (11) can be written in its normal form by rotating the axes X, Y, and Z to the corresponding principal axes X', Y', and Z' at an angle that eliminates the cross terms. Applying the rotation

$$\begin{bmatrix}X\\ Y\\ Z\end{bmatrix} = \begin{bmatrix}\cos\theta & 0 & \sin\theta\\ 0 & 1 & 0\\ -\sin\theta & 0 & \cos\theta\end{bmatrix}\begin{bmatrix}X'\\ Y'\\ Z'\end{bmatrix} \tag{12}$$

to Eq. (11), the following result is obtained:

$$\begin{aligned}&(\eta_1\cos^2\theta + \eta_3\sin^2\theta - \eta_5\sin 2\theta)X'^2 + \eta_2 Y'^2\\ &+ (\eta_1\sin^2\theta + \eta_3\cos^2\theta + 2\eta_5\cos 2\theta)Z'^2\\ &+ (\eta_1\sin 2\theta - \eta_3\sin 2\theta + 2\eta_5\cos 2\theta)X'Z' = 1\end{aligned} \tag{13}$$

and Eq. (13) is transformed to the normal ellipsoid form by choosing θ so that the coefficient of the cross term $X'Z'$ is zero, i.e.,

$$\theta = \frac{1}{2}\arctan\left(\frac{-2\eta_5}{\eta_1 - \eta_3}\right). \tag{14}$$

The resulting normal form of Eq. (13) yields the following expressions for the refractive indices in the principal directions X', Y', and Z':

$$\begin{aligned}n_{X'} &= 1/\sqrt{\eta_1\cos^2\theta + \eta_3\sin^2\theta - \eta_5\sin 2\theta},\\ n_{Y'} &= \frac{1}{\eta_2},\\ n_{Z'} &= 1/\sqrt{\eta_1\sin^2\theta + \eta_3\cos^2\theta - \eta_5\sin 2\theta}.\end{aligned} \tag{15}$$

Single-crystal paratellurite (TeO_2) is generally used as an acousto-optic material because of its good photoelastic properties and transparency over a broad wavelength ranging from 0.35 to 5 μm [18,25]. However, TeO_2 is an anisotropic acousto-optic material both optically and acoustically. For the wavelength 632.8 nm in vacuum and TeO_2 at room temperature, the ordinary and extraordinary refractive indices [24]

are $n_o = 2.26$ and $n_e = 2.41$, respectively. The photoelastic coefficients for this material are reported as [26]

$$[p_{ij}] = \begin{bmatrix} p_{11} & p_{12} & p_{13} & 0 & 0 & 0 \\ p_{12} & p_{11} & p_{13} & 0 & 0 & 0 \\ p_{31} & p_{31} & p_{33} & 0 & 0 & 0 \\ 0 & 0 & 0 & p_{44} & 0 & 0 \\ 0 & 0 & 0 & 0 & p_{44} & 0 \\ 0 & 0 & 0 & 0 & 0 & p_{66} \end{bmatrix}, \quad (16)$$

with $p_{11} = 0.0074$, $p_{12} = 0.187$, $p_{13} = +0.340$, $p_{31} = +0.0905$, $p_{33} = +0.240$, $p_{44} = -0.170$, and $p_{66} = -0.0463$. In this study, the refractive index of the material at unstrained condition is taken as $n_u = \sqrt{n_o n_e}$ in Eq. (11). To calculate the refractive index modulation $\Delta n(x, z)$, the strain in the AOD medium is calculated using Eq. (6), for which the atomic displacement vector, $\bar{U}(x, z) = \hat{i}u_i + \hat{j}u_j$, is obtained using Eq. (1). The strain tensor S_{ij} and the photoelastic coefficients of Eq. (16) were applied to Eq. (9) to determine different components of the impermeability tensor $\eta_1, \eta_2, \ldots, \eta_6$, which were substituted into Eq. (15) to calculate. The refractive indices in the x and z directions, $n_{X'}$ and $n_{Z'}$. Since the transducers are infinitely long in the y direction, the ultrasonic waves induce two-dimensional strains in the x–z plane. Consequently, two principal values of the refractive index, $n_{X'}$ and $n_{Z'}$, in the principal directions X' and Z', respectively, are different from the unstrained refractive index n_u, and the third principal value, $n_{Y'}$, is the same as n_u. A mean value of the refractive index can be calculated as $n_s = \sqrt{n_{X'} n_{Z'}}$ for the strained AOD under the quasi-isotropic approximation, which generally holds good for weakly anisotropic media [27]. The two-dimensional change in the refractive index compared to the unstrained AOD is determined as $\Delta n(x, z) = n_s(x, z) - n_u(x, z)$.

3. RESULTS AND DISCUSSION

Results are obtained for TeO_2 as the AOD medium using the refractive index data at the He–Ne laser wavelength of 632.8 nm in vacuum. The speeds of ultrasonic L-waves and S-waves in this material are 4202 ± 10 m/s and 616 ± 10 m/s, respectively, for a piezoelectric transducer operating at 75 MHz [17], which yields the acoustic wavelength $\Lambda = 56$ μm and the acoustic wave number $\kappa = 1.12 \times 10^5$ m^{-1} inside the AOD medium. In this study, the attenuation coefficient of the ultrasonic wave is taken as $\alpha = 0$, and the distance for the point of focus is taken as $F' = 10^6$ mm to determine the phase shift or time delay using Eq. (5) for different values of the steering angle θ_s. The half-width, a, and pitch of the transducers are 10.4 and 28 μm, respectively. The amplitude of the ultrasonic waves emitted by each transducer is taken to be $P_0 = 1$ N/mm^2 for the following results unless stated otherwise.

The phased array transducer in this study is a row of 22 planar transducers with the central operating frequency of 75 MHz. The pitch of the array is $S = \Lambda/2$, and the width of each element is $W = 0.742S$. The formation of grating lobes is avoided by choosing the difference of the time delay between two adjacent transducers as an integral multiple of half-wavelength, i.e., the pitch $S = \Lambda/2$.

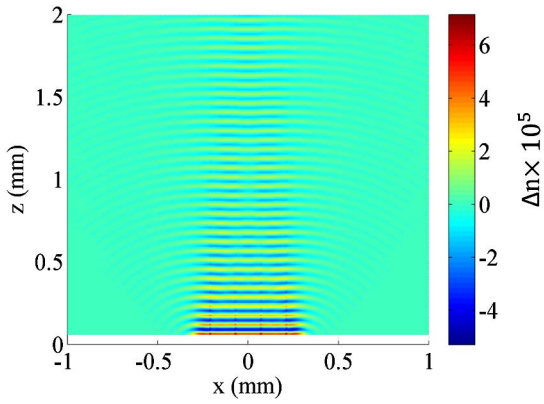

Fig. 2. Two-dimensional strain-induced index change of Δn with the beam steering angle of $\theta_s = 0°$.

Figures 2 and 3 show the strain-induced two-dimensional index change in a rectangular region of 2 mm × 2 mm for the beam steering angles $\theta_s = 0°$ and 30°, respectively. These two angles correspond to the time delays $\Delta\tau = 0$ and 3.33 s, respectively. In Fig. 2, the ultrasonic waves, which are emitted by each transducer, propagate vertically upward while spreading laterally due to diffraction. Consequently, the overlapping waves interfere to produce a composite wave field in the form of a diffraction pattern. This pattern, therefore, defines the strain field within which the refractive index is modified. The refractive index varies in the z and x directions due to longitudinal and lateral strains in the vertical and horizontal directions, respectively. For Fig. 3, on the other hand, the time delay was so selected that the composite wave field is steered at a certain angle and, therefore, the refractive index pattern is also tilted. These results indicate that the index pattern can be oriented in different directions by varying $\Delta\tau$ to produce a dynamic phase grating in the AOD medium for deflecting laser beams at large angles.

The two-dimensional features of the index change, $\Delta n(x, z)$, are examined in Figs. 4 and 5 and represent the front and rear views of the index profile, respectively, when

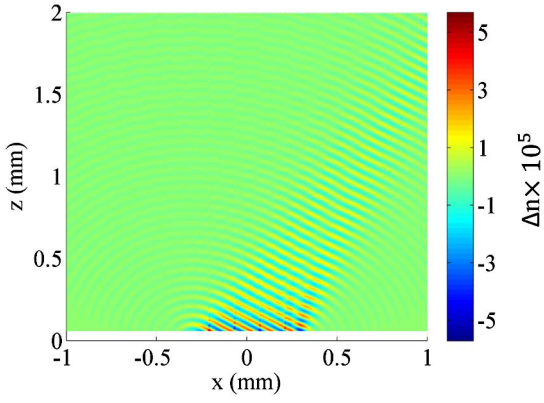

Fig. 3. Two-dimensional strain-induced index change of Δn with the beam steering angle of $\theta_s = 30°$.

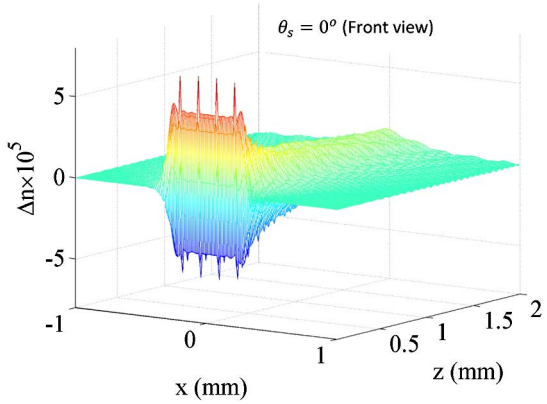

Fig. 4. Three-dimensional strain-induced index change with the beam steering angle of $\theta_s = 0°$.

the acoustic beam steering angle $\theta_s = 0°$ and each transducer emits the acoustic waves as a rectangle function. Near the transducer plane, the composite acoustic wavefront assumes a rectangular diffraction pattern of peak intensity at the two edges of the rectangle and oscillating intensity of very small amplitude between the edges. This type of pattern is formed due to Gibbs' phenomenon in the Fourier series representation of rectangle functions. Due to this acoustic diffraction pattern, the refractive index has a rectangular profile near the transducer plane as shown in Fig. 4.

However, the diffraction pattern assumes the Fresnel and Fraunhofer patterns slightly away and far away from the transducer plane, respectively, since the waves spread in the longitudinal and transverse directions. Consequently, the index profile also changes as indicated by the rear view of the index surface in Fig. 5. One of the attractive features of phased array transducers is their capability of dynamic index modulation steering that does not require mechanical scanning.

The effects of transducers having different central RF frequencies, 59, 75, and 91 MHz, are presented in Figs. 6–8, respectively, for different steering angles. These results show the periodic variation, i.e., the amplitude and wavelength, of Δn along the beam steering axis z_s. The steering angles do not affect the wavelength since it is determined by the central

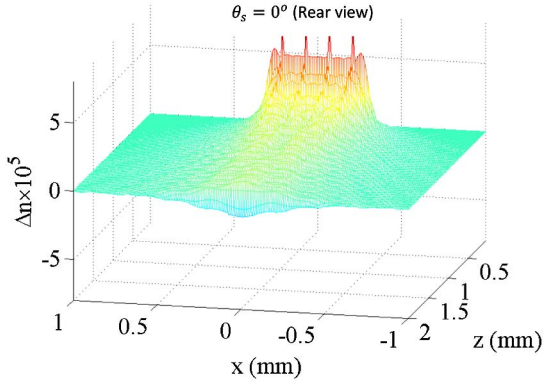

Fig. 5. Three-dimensional strain-induced index change with the beam steering angle of $\theta_s = 0°$.

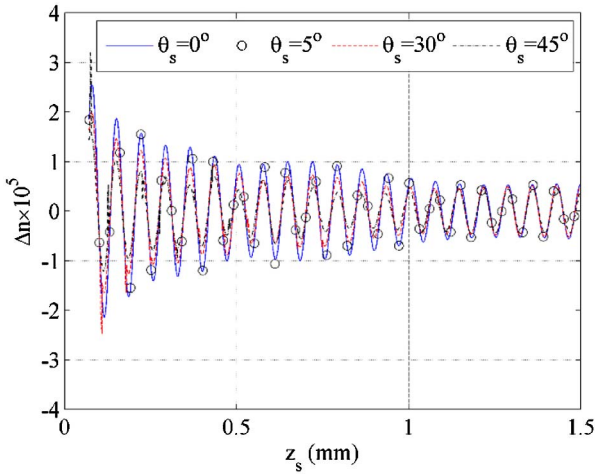

Fig. 6. One-dimensional strain-induced index change along beam steering axis at center RF frequency of $F_c = 59$ MHz with varying steering angle of $\theta_s = 0°$, 5°, 30°, and 45°.

RF frequency. Based on the acoustic frequency and velocity, the wavelengths of the acoustic waves in the AOD medium are 71, 56, and 46 μm at $F = 59$, 75, and 91 MHz, respectively, and the corresponding periodicities of the index modulation are found to be 71.4, 55.6, and 45.5 μm along the beam steering axis. This reduction in the periodicity of Δn is because the wavelength is inversely proportional to the frequency. At a fixed RF frequency, the steering angle does not affect the periodicity of the index modulation, but the amplitude decreases as the angle increases. The reductions in the amplitude due to the beam steering angle of 45° compared to the zero steering angle are 41% and 38% in the near and far fields, respectively. Figures 6–8 show that the refractive index modulation (Δn) increases as the RF frequency increases, which is because the wave number, κ, increases as the frequency increases. The mechanical displacement vector of the atoms, on the other hand, is affected by the wave number as indicated by Eqs. (1) and (2), and consequently the

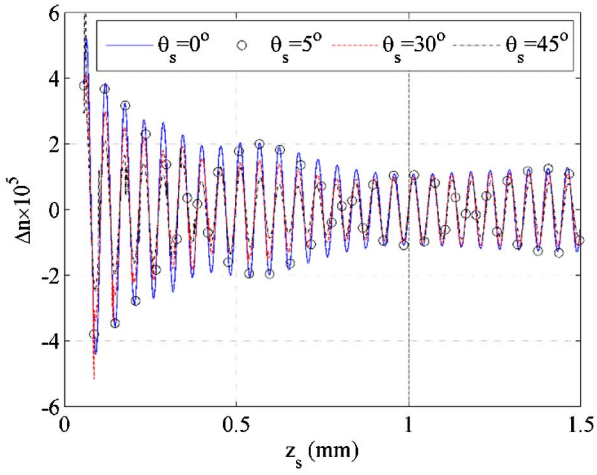

Fig. 7. One-dimensional strain-induced index change along beam steering axis at center RF frequency of $F_c = 75$ MHz with varying steering angle of $\theta_s = 0°$, 5°, 30°, and 45°.

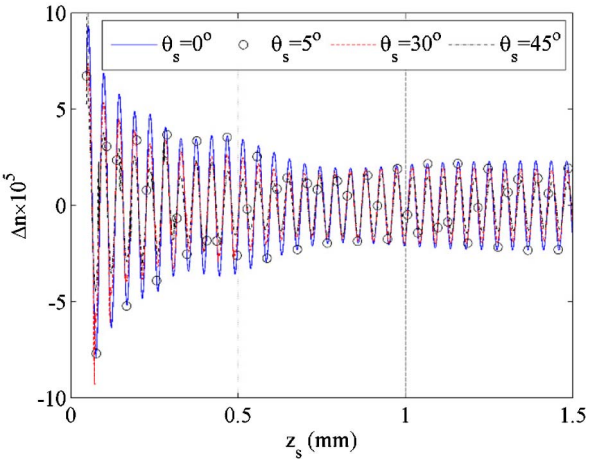

Fig. 8. One-dimensional strain-induced index change along beam steering axis at center RF frequency of $F_c = 91$ MHz with varying steering angle of $\theta_s = 0°$, 5°, 30°, and 45°

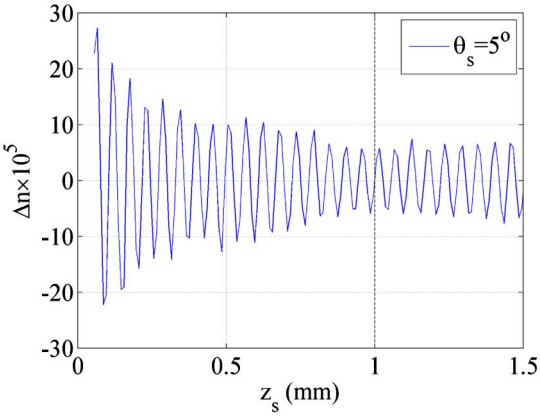

Fig. 10. One-dimensional strain-induced index change along beam steering axis at center RF frequency of $F_c = 75$ MHz with varying steering angle of $\theta_s = 5^o$ with left-half pressure of $P_0 = 1$ N/mm^2 and right-half pressure of $P_0 = 10$ N/mm^2.

strain depends on the frequency. It is also known that Δn depends on the strain as indicated by Eq. (7). Therefore Δn varies with frequency through the strain term.

The effects of different pressures exerted on the AOD medium by the acoustic waves are studied in Figs. 9 and 10. For the results in both figures, the pressure exerted by each of the left-half 11 transducers, which lie on the $-x$ axis, is $P_0 = 1$ N/mm^2. The pressures exerted by each of the right-half 11 transducers, which lie on the $+x$ axis, are $P_0 = 0.1$ N/mm^2 and 10 N/mm^2 for Figs. 9 and 10, respectively. Higher pressure would increase the amplitude of the acoustic waves, resulting in more strain in the AOD medium and, consequently, large modulation in the refractive index. This phenomenon can be observed in Figs. 9 and 10, which show that Δn is much higher in Fig. 10 due to higher right-half pressure than that in Fig. 9.

Different acoustic pressures imply different amplitudes of the acoustic waves, and, therefore, the intensity distribution in the diffraction pattern of these waves can be manipulated using the pressure in addition to the phase of the waves. For example, two waves of π-phase shift but different amplitudes will not create null intensity in the diffraction pattern. Thus operating the transducers at different pressures provides an additional mechanism to control the quality of the phase grating; i.e., Δn can be varied sharply or diffusely by modifying the intensities in the constructive and destructive interference fringes of the pattern. The acoustic pressure, however, depends on the RF power, and the diffraction efficiency of AOD attains a maximum value at an optimal RF driving power. Therefore, excessive acoustic pressure can lower the diffraction efficiency even though Δn is large.

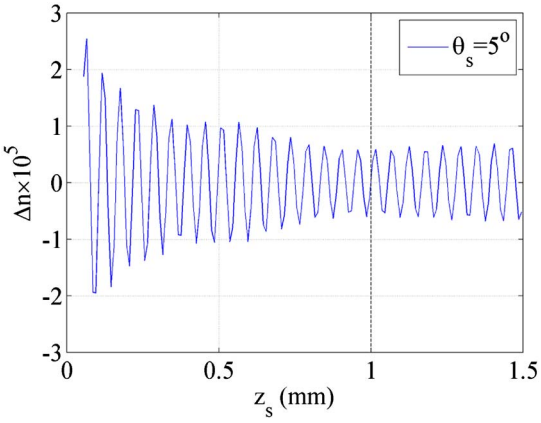

Fig. 9. One-dimensional strain-induced index change along beam steering axis at center RF frequency of $F_c = 75$ MHz with varying steering angle of $\theta_s = 5^o$ with left-half pressure of $P_0 = 1$ N/mm^2 and right-half pressure of $P_0 = 0.1$ N/mm^2.

4. CONCLUSIONS

A mathematical model is presented for generating dynamic phase gratings in AOD media based on strain-induced modulation of two-dimensional refractive index. Phased array transducers enable acoustic beam steering at any arbitrary angle, and this steering effect is utilized to tilt the modulated index profile that can be implemented in AOD devices for deflecting laser beams at large angles. The shape of the index profile and the magnitude of the change in the index are significantly different near the transducer plane compared to far away regions. While the periodicity of the index modulation is determined by the central RF frequency of the transducers, the amplitude of the index modulation is found to decrease as the steering angle increases. The acoustic pressure affects the amplitude of the index profile significantly, yielding higher amplitudes at higher pressures.

Funding. Semiconductor Research Corporation (SRC); Intel Corporation.

REFERENCES

1. M. Gottlieb, C. L. M. Ireland, and J. M. Ley, "Scanning systems," in *Electro-Optic and Acousto-Optic Scanning and Deflection* (Marcel Dekker, 1983), pp. 158–174.
2. A. P. Goutzoulis and V. V. Kludzin, "Principles of acousto-optics," in *Design and Fabrication of Acousto-Optic Devices*, A. P. Goutzoulis and D. R. Pape, eds. (Marcel Dekker, 1994), pp. 1–69.

3. E. H. Young and H. C. Ho, "Acousto-optic device technology: design," in *Acousto-Optic Signal Processing: Theory and Implementation*, N. J. Berg and J. M. Pellegrino, eds., 2nd ed. (Dekker, 1996), pp. 47–80.
4. G. Aubin, J. Sapriel, V. Y. Molchanov, R. Gabet, P. Grosso, S. Gosselin, and Y. Jaouen, "Multichannel acousto-optic cells for fast optical crossconnect," Electron. Lett. **40**, 448–449 (2004).
5. S. N. Antonov and Y. G. Rezvov, "Efficient multi-beam Bragg acousto-optic diffraction with phase optimization of a multifrequency acoustic wave," Tech. Phys. **52**, 1053–1060 (2007).
6. L. Zhao, Q. Zhao, J. Zhou, S. Tian, and H. Zhang, "Two-dimensional multi-channel acousto-optic diffraction," Ultrasonics **50**, 512–516 (2010).
7. K. C. Vermeulen, J. van Mameren, G. J. M. Stienen, E. J. G. Peterman, G. J. L. Wuite, and C. F. Schmidt, "Calibrating bead displacements in optical tweezers using acousto-optic deflectors," Rev. Sci. Instrum. **77**, 013704 (2006).
8. A. E. Wallin, H. Ojala, E. Hæggström, and R. Tuma, "Stiffer optical tweezers through real-time feedback control," Appl. Phys. Lett. **92**, 224104 (2008).
9. A. H. Mack, M. K. Trías, and S. G. J. Mochrie, "Precision optical trapping via a programmable direct-digital-synthesis-based controller for acousto-optic deflectors," Rev. Sci. Instrum. **80**, 016101 (2009).
10. V. Iyer, T. M. Hoogland, and P. Saggau, "Fast functional imaging of single neurons using random-access multiphoton (RAMP) microscopy," J. Neurophysiol. **95**, 535–545 (2005).
11. Y. Kremer, J.-F. Léger, R. Lapole, N. Honnorat, Y. Candela, S. Dieudonné, and L. Bourdieu, "A spatio-temporally compensated acousto-optic scanner for two-photon microscopy providing large field of view," Opt. Express **16**, 10066–10076 (2008).
12. P. A. Kirkby, K. M. N. Srinivas Nadella, and R. A. Silver, "A compact acousto-optic lens for 2D and 3D femtosecond based 2-photon microscopy," Opt. Express **18**, 13720–13744 (2010).
13. S. Dupont and J.-C. Kastelik, "Wide-band acousto-optic deflectors with high efficiency for visible range fringe pattern projector," Rev. Sci. Instrum. **78**, 105102 (2007).
14. S. Dupont and J.-C. Kastelik, "Demonstration of a tunable two-frequency projected fringe pattern with acousto-optic deflectors," Rev. Sci. Instrum. **79**, 056101 (2008).
15. S. Dupont, J.-C. Kastelik, and M. Pommeray, "Structured light fringe projection setup using optimized acousto-optic deflectors," IEEE/AMSE Trans. Mechatron. **15**, 557–560 (2010).
16. M. G. Gazalet, M. Ravez, F. Haine, C. Bruneel, and E. Bridoux, "Acousto-optic low-frequency shifter," Appl. Opt. **33**, 1293–1298 (1994).
17. C. Grebing, S. Koke, and G. Steinmeyer, "Self-referencing of optical frequency combs," in *Conference on Lasers and Electro-Optics/International Quantum Electronics Conference*, OSA Technical Digest (Optical Society of America, 2009), paper CTuK5.
18. J. Xu and R. Stroud, "Crystal optics and acoustics," in *Acousto-Optic Devices: Principles, Design, and Applications* (Wiley, 1992), pp. 32–42.
19. K. Nakahata and N. Kono, "3-D modelings of an ultrasonic phased array transducer and its radiation properties in solid," in *Ultrasonic Waves*, A. A. dos Santos, ed. (InTech, 2012), pp. 59–80.
20. T. Wang, C. Zhang, A. Aleksov, I. Salama, and A. Kar, "Two-dimensional analytic modeling of acoustic diffraction for ultrasonic beam steering by phased array transducers," Ultrasonics **76**, 35–43 (2017).
21. M. G. Silk, "Ultrasonic beam modification techniques for piezoelectric probes," in *Ultrasonic Transducers for Nondestructive Testing* (Adam Hilger, 1984), pp. 90–93.
22. J. M. Liu, "Acousto-optic devices," in *Photonic Devices* (Cambridge University, 2005), pp. 357–363.
23. A. Yariv and P. Yeh, "Acousto-optics," in *Optical Waves in Crystals* (Wiley, 1984), pp. 318–365.
24. J. C. Kastelik, M. G. Gazalet, C. Bruneel, and E. Bridoux, "Acoustic shear wave propagation in Paratellurite with reduced spreading," J. Appl. Phys. **74**, 2813–2817 (1993).
25. N. Uchida and N. Niizeki, "Acoustooptic deflection materials and techniques," Proc. IEEE **61**, 1073–1092 (1973).
26. N. Uchida and Y. Ohmachi, "Elastic and photoelastic properties of TeO_2 single crystal," J. Appl. Phys. **40**, 4692–4695 (1969).
27. A. A. Fuki, Y. A. Kravtsov, and O. N. Naida, "Geometrical optics of inhomogeneous media," in *Geometrical Optics of Weakly Anisotropic Media* (Gordon and Breach Science, 1998), p. 26.